2003-01-0937

Impact of the inlet flow distribution on the light-off behavior of a 3-way catalytic converter

Julia Windmann, Joachim Braun, Peter Zacke
J. Eberspächer GmbH & Co. KG

Steffen Tischer, Olaf Deutschmann, Jürgen Warnatz
University of Heidelberg

ABSTRACT

Numerical simulations are increasingly assisting research and development in the field of emission control of automotive vehicles.

Our work focuses on the prediction of the tail-pipe emissions, based on a numerical simulation of the automotive catalytic converter. Besides the prediction of the tail-pipe emissions, an understanding of the processes occurring inside a monolithic catalytic converter implies new opportunities for the design of the optimum exhaust gas system.

In this paper, we present a three-dimensional transient numerical study of the influence of the velocity distribution in front of the inlet face on the thermal behavior of the monolith during the light-off of a 3-way catalytic converter. The differences in the thermal and chemical behavior due to the shape of the velocity distribution are discussed.

The recently developed code DETCHEM^{MONOLITH} /1/ is used for the numerical simulation. This code, for the first time, combines two-dimensional simulations of the reactive flow inside a large number of single monolith channels including a heterogeneous multi-step reaction mechanism with a transient simulation of the three-dimensional temperature field of the entire converter.

INTRODUCTION

The conversion efficiency and light-off of a catalytic converter depends on various factors. On one hand, there are the properties of the monolith such as cross section, length, cell density, wall thickness, washcoat and coating. On the other hand, the flow characteristics of the exhaust gas such as flow velocity, temperature, composition of raw emissions and flow distribution play an important role for the conversion rate and the light-off. These factors also have an influence on the ageing of the catalytic converter /2//3/.

In this paper we will focus on the impact of the flow distribution on the conversion rate and light-off behavior of the catalytic converter. It is well-known that a velocity maldistribution can lead to an uneven heat distribution in the monolith. Thus, the monolith heats up slower in zones with a lower flow velocity and as a result the light-off is delayed. The pollutants entering these zones pass the monolith unconverted and the overall conversion is decreased. Here, we will illustrate this effect by a very detailed numerical simulation of the physical, chemical and thermal processes occurring in the catalytic converter.

In contrast to the wide variety of studies on reactive flows in single channels, there has been a relatively small number of sophisticated models for the simulation of the entire catalytic monolith using simultaneously detailed models of transport and chemistry in the single channels. Significant contributions have been made by Kolaczkowski, Hayes and co-workers /4/–/7/. A transient 3D-model of a monolith including 24 parallel channels has been proposed by Marek and co-workers, which applies a plug-flow model for the transport in the single channels and a single-step surface reaction /8/. Koltsakis et al. /9/ used a transient two-dimensional description of the solid structure of the monolith coupled with a simplified model of the channels' flow fields including a multi-step surface reaction mechanism and a oxygen-storage model.

Recent publications /10/,/11/ have shown the potential of DETCHEM^{MONOLITH} to simulate the transient behavior of catalytic, monolithic reactors and converters with various complex inlet and boundary conditions. The code, for the first time, combines two-dimensional parabolic simulations of the reactive flow inside a large number of single monolith channels including multi-step homogeneous and heterogeneous reaction mechanisms with a transient simulation of the three-dimensional temperature field of the entire monolith. Furthermore, the code can additionally apply washcoat models based on either an effectiveness factors (simple model) or a set of one-dimensional reaction-diffusion equations, which

spatially resolve species profiles and surface coverages inside the washcoat layer.

In our former study /10/ only a uniform velocity distribution at the inlet face of the converter was considered. Now we will reveal the differences between an even and an uneven flow distribution in front of the catalytic converter in detail.

MATHEMATICAL AND NUMERICAL MODEL

The numerical model for the simulation of the monolith is based on the same assumptions as described before /10/, i.e., the time scale of the reactive flow through single channels of the catalytic converter is regarded to be much faster than the thermal response of the monolith's solid. Then fluctuations in the monolith temperature can be neglected when calculating the fluid flow through a single channel. Thus, a time independent formulation is used to describe the gaseous flow in order to calculate heat source terms for a transient heat conduction equation for the solid /12/.

The program DETCHEM^{CHANNEL} /1/ is used to solve the laminar time-independent boundary-layer equations of a fluid flow through a cylindrical channel. In comparison to the Navier-Stokes equations, the diffusion terms along the direction of convection are neglected. This model has been proven useful for higher flow velocities /13/, as they are expected in this application. In case of a turbulent flow entering the single channel, the parabolic laminar flow profile will quickly be established due to the small channel diameter and low Reynolds number. This entrance effect is modeled by applying a uniform velocity profile at the entrance. If the physical conditions lead to a fully developed turbulent flow enhancing mixing, a plug-flow model may be used as simplified model /13/ or a turbulence model has to be added to the equation system as described in, e.g., /13/.

The equations to be solved are:

Conservation of total mass

$$\frac{\partial(r\rho u)}{\partial z}+\frac{\partial(r\rho v)}{\partial r}=0\ , \tag{1}$$

Conservation of species mass

$$\frac{\partial(r\rho u Y_i)}{\partial z}+\frac{\partial(r\rho v Y_i)}{\partial r}=-\frac{\partial}{\partial r}(r j_i)\ , \tag{2}$$

Conservation of axial momentum

$$\frac{\partial(r\rho u u)}{\partial z}+\frac{\partial(r\rho v u)}{\partial r}=-r\frac{\partial p}{\partial z}+\frac{\partial}{\partial r}\left(\mu r\frac{\partial u}{\partial r}\right), \tag{3}$$

And conservation of enthalpy

$$\frac{\partial(r\rho u h)}{\partial z}+\frac{\partial(r\rho v h)}{\partial r}= ru\frac{\partial p}{\partial z}+\frac{\partial}{\partial r}\left(\lambda r\frac{\partial T}{\partial r}\right)-\frac{\partial}{\partial r}\left(\sum_i r j_i h_i\right) \tag{4}$$

All transport coefficients depend on temperature and composition. The boundary conditions for these equations are the wall temperature profile and the conditions (mass, momentum and enthalpy flux) at the inlet of the channel, which can be calculated from velocity, temperature and composition of the gas.

Despite the actual shape of the channels, a cylindrical model is used in order to reduce the numerical complexity. Nevertheless, variations in the washcoat thickness compensate the deviations in shape.

Catalytic reactions at the surface are taken into account in terms of the diffusive mean flux j_i at the gas-phase/washcoat interface in Equ. (2)

$$j_{i,surf}=\eta F_{cat/geo} M_i \dot{s}_i\ . \tag{5}$$

The effect of the washcoat is described by the factor η, which includes a washcot diffusion model, and the surface scaling factor $F_{cat/geo}$. The reaction-rate expressions $\dot{s}_i$ use a detailed surface reaction mechanism accounting for varying surface coverages Θ_i

$$\dot{s}_i=\sum_{k=1}^{K_s}\nu_{ik}k_{fk}\prod_{j=1}^{N_g+N_s}c_j^{\nu'_{jk}}\ , \tag{6}$$

with rate coefficient

$$k_{fk}=A_k T^{\beta_k}\exp\left[\frac{-E_{ak}}{RT}\right]f_k\left(\Theta_1,\mathrm{K},\Theta_{N_s}\right) \tag{7}$$

and coverage dependency function

$$f_k\left(\Theta_1,\mathrm{K},\Theta_{N_s}\right)=\prod_{i=1}^{N_s}\Theta_i^{\mu_{ik}}\exp\left[\frac{\varepsilon_{ik}\Theta_i}{RT}\right]. \tag{8}$$

The boundary-layer equations can be solved in a single sweep of integration along the axial direction by a method-of-lines procedure using an adaptive integration step size. The radial derivatives are discretized using a finite-volume method. The resulting differential-algebraic equation system is integrated using the semi-implicit extrapolation solver LIMEX /15/.

Using this steady-state channel model, a transient simulation of the thermal behavior of the entire monolith is performed by DETCHEM^{MONOLITH} /1/. The solid's

temperature field is described by a three-dimensional conservation equation

$$\frac{\partial T_{monolith}}{\partial t} = \nabla^2 \left(\frac{\lambda T_{monolith}}{\rho\, c_p} \right) + \frac{q}{\rho\, c_p} \quad . \tag{9}$$

The material properties (density ρ, heat capacity c_p and thermal conductivity λ) are functions of the local temperature and material (monolith, insulation and canning). The thermal conductivity also depends on the direction (axial or radial). Due to the structure, the effective thermal conductivity may also vary with the direction relative to the channels. Boundary conditions may be of Dirichlet or Neumann type including convection and radiation.

The source term q describes the coupling between the gas and the solid phase. It is calculated by DETCHEM^{CHANNEL} as:

$$q = -\sigma \cdot 2\pi r\, \lambda \left. \frac{\partial T_{gas}}{\partial r} \right|_{surface} \quad . \tag{10}$$

Here is assumed that the monolith can be regarded as a continuum with an averaged cross-sectional channel density σ.

For each time step and discretized spatial coordinate the quasi-steady-state source term can be calculated by DETCHEM^{CHANNEL}. Therefore DETCHEM^{MONOLITH} provides the inlet and boundary conditions, i.e. the channel wall temperature equals the monolith temperature at the corresponding point. So each axial row of monolith cells together with the inlet conditions at that cross-sectional position defines one set of parameters for distinguished channels. The number of channels to be simulated for each time step increases with the number of inlet face points. However, the detailed simulation of the fluid flow through a channel is the most time-consuming step in this model. Therefore only a representative set of channels is simulated using DETCHEM^{CHANNEL}.

The representative channels are chosen through a cluster-analysis algorithm. The sets of inlet conditions and wall temperature profiles of all channels are compared. If two of them do not differ by a specified difference in any temperature and by a given percentage in the inlet velocity, they are represented by the same averaged set of conditions. Further, channels that were simulated once can be stored and then they are used in successive time-steps in case they represent another cluster of channels.

COUPLING TO THE TAIL-PIPE FLOW

The code DETCHEM^{MONOLITH} can be linked to steady-state or transient, spatially uniform or varying inlet conditions. Those data can be given manually in tabular form or as CFD simulation results. If transient CFD simulation results for the up-stream part of the exhaust gas system exist, data sets containing the normal velocity, gas phase temperature and species concentrations at the inlet face can be used as input data for DETCHEM^{MONOLITH} directly. At present an inlet filter for data provided in Tecplot® /16/ format is available. Data from the CFD code FLUENT /17/ can also be used by exporting them to the Tecplot® data format.

CHEMICAL REACTION SYSTEM

A detailed multi-step reaction mechanism is used to model the catalytic reactions in a three-way catalytic converter that contains Pt and Rh as active catalysts.

In this simulation only surface chemistry is included; gas phase chemistry can be neglected because of the low pressure and temperature, and the short residence time. The sample exhaust gas mixture is composed of C_3H_6, CH_4, CO_2, H_2O, CO, NO, O_2, N_2. The surface reaction scheme consists of 62 reaction steps among these eight gas-phase and further 29 adsorbed chemical species. It is assumed that all species are adsorbed competitively. The model also considers the different adsorption sites (platinum or rhodium) of the surface. However, on rhodium, surface reactions are considered between NO, CO, and O_2 only. The kinetic data of the mechanism were taken either from literature or fits to experimental data. The mechanism is based on our former studies and are described in more detail in /18/.

The parameters of the catalyst used, e.g., metal composition and loading, dispersion, have taken as described before /10/. In the simulation, a simplified washcoat model is used with CO as species that determines the effectiveness factor η. /2//18/.

CONFIGURATION AND CONDITIONS

GEOMETRY

For the simulations a commercially available three-way catalytic converter with a circular cross-section was assumed. The specifications of the substrate, the coating and the canning are listed in Tab. 1.

Substrate

Material	Cordierit	
Diameter	$85.9 \cdot 10^{-3}$ m	(3.38")
Length	$57.2 \cdot 10^{-3}$ m	(2.25")
Cell density	62 cm^{-2}	(400 cpsi)
Wall thickness	$1.525 \cdot 10^{-4}$ m	(6 mil)

Coating

Pt : Rh	5 : 1
Loading	80 g/ft^3

Canning

Thickness of supporting mat	$4.2 \cdot 10^{-3}$ m
Metal thickness	$1.5 \cdot 10^{-3}$ m

Tab. 1 Specifications of the catalytic converter

The numerical representation of the catalytic converter is illustrated in Fig. 1.

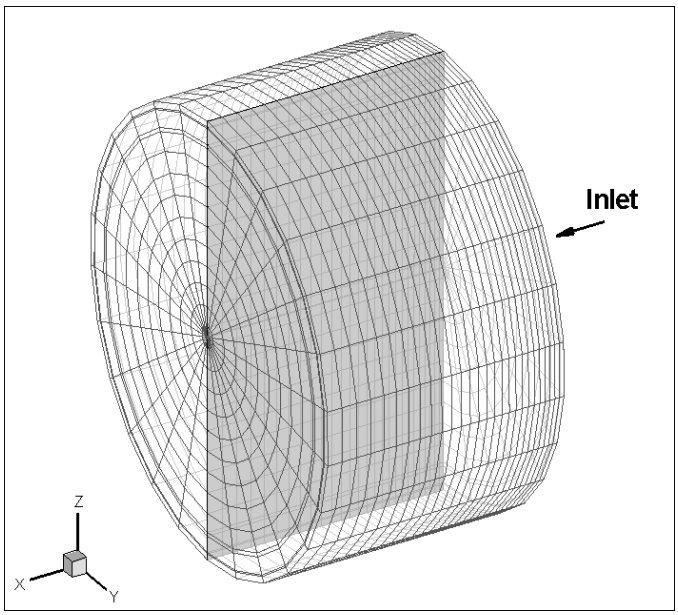

Fig. 1: The three-dimensional numerical grid.
The flow runs in the positive x-direction

INLET AND BOUNDARY CONDITIONS

As inlet conditions data from an engine test bench experiment were chosen. In this experiment the engine was run in the ECE and EUDC cycles mode.

In Fig. 2 and Fig. 3 the resulting temperatures and gas phase velocities in front of the catalytic converter are shown. In both plots the range of the first 100 seconds is exposed.

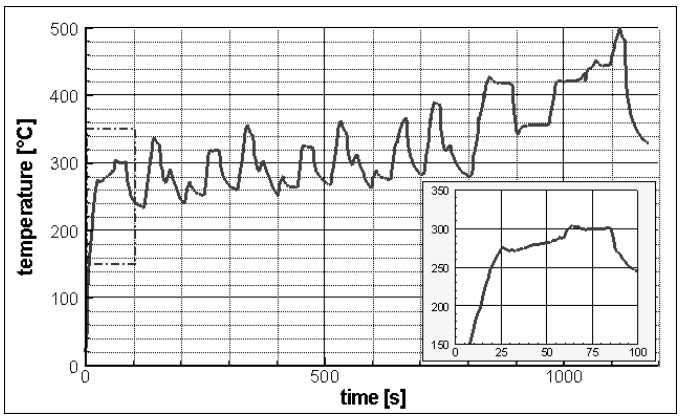

Fig. 2 Inlet gas phase temperature;
the range of the first 100 seconds is shown in detail.

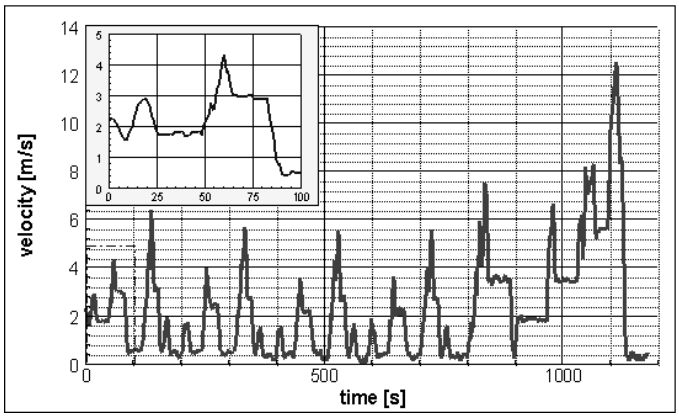

Fig. 3 Inlet gas phase velocity;
the range of the first 100 seconds is shown in detail.

As the impact of the inlet flow distribution on the conversion rate shall be examined, two different inlet flow profiles were chosen as boundary conditions:

- a uniform velocity profile and
- an uneven velocity profile shown in Fig. 4.

Uniform velocity profile

In the case of the uniform velocity profile it is assumed that at every position on the inlet face the exhaust gas enters the monolith with the mean velocity of each time step. The increase of the gas phase velocity due to the decrease of the free cross-section in the monolith is taken into account.

Non-uniform velocity profile

In order to examine the impact of an uneven velocity distribution on the light-off behavior of the catalytic converter the profile shown in Fig. 4 is used as inlet velocity distribution. This was calculated by a general purpose CFD code in which the monolith was modeled as a porous media. Although it was possible to vary the velocity distribution according to the mass flow rate, for simplification it is assumed that this velocity distribution

is valid for all time steps. The authors are aware that this assumption is a strong simplification of the real flow conditions in an exhaust gas system. Nevertheless in order not to mingle the impact of different effects, it is assumed that the velocity distributions are qualitatively invariable. The normalized distribution (with a mean velocity of 1 m/s) is multiplied with the mean velocity of each time step. For the quantification of the uniformity of the velocity distribution, the uniformity index γ

$$\gamma = 1 - \frac{1}{2 \cdot A} \cdot \int \left| \frac{w}{\overline{w}} - 1 \right| \cdot dA \qquad (11)$$

is usually used. For the given velocity distribution this index was determined to be $\gamma = 0.58$.

The increase of the gas phase velocity in the monolith due to the open frontal area (OFA) of the substrate is again directly taken into account by the simulation code.

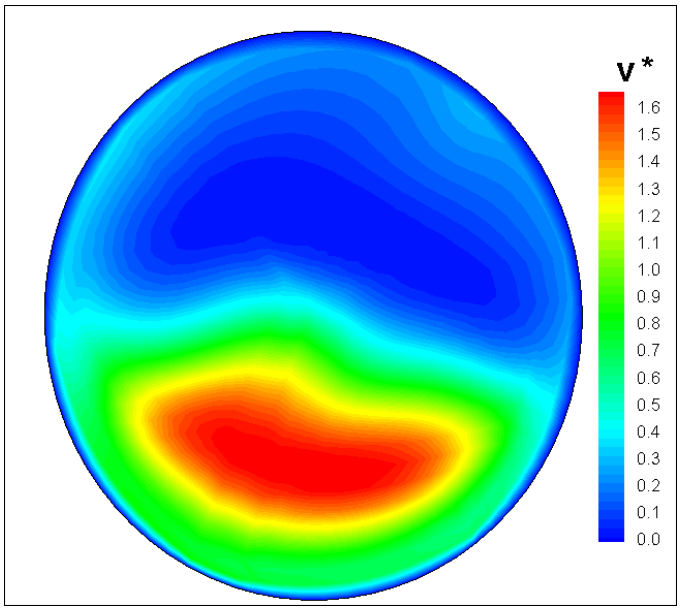

Fig. 4 Normalized velocity distribution at the inlet

Temperature and species concentrations

Despite the profile of the inlet velocity, it is assumed that the inlet temperature and species concentration distribution is uniform.

The input species concentrations were chosen according to the experimental data measured during the experiments at the engine test bench. Due to the fact that the experiments were not originally intended to gain emission data, only catalytically inactive substrates were installed. The measured species concentrations were prepared for the simulations as described in /10/.

Thermal boundary conditions

At the exterior walls of the catalytic converter heat transfer due to thermal convection and radiation was taken into account. The emissivity of the external surface of the catalytic converter was assumed as 0.8. Convection was taken into account by a heat transfer coefficient of 80 W/(m^2 K).

RESULTS AND DISCUSSION

In the following figures, results from various simulations are shown. One simulation was set up with the uniform velocity distribution at the inlet. For three simulations the inlet velocity distribution shown in Fig. 4 was used. In these simulations the clustering parameters for the choice of the representative channels were varied between 10 and 30 K for temperature and 10 and 50 percent for the inlet velocity. This led to different numbers of channels, that were calculated at each time step: with the most stringent parameters (3D-profil-1) up to 98 channels were simulated, with more relaxed parameters up to 45 channels (3D-profil-2) and 35 channels (3D-profil-3) were considered at different time steps.

As this paper focuses on the light-off behavior of the catalytic converters, only the initial phase of the test cycle will be examined and discussed.

GLOBAL OUTLET TEMPERATURE

Fig. 5 depicts the inlet and the calculated averaged outlet gas phase temperatures during the first 80 s. Already after 5 seconds the simulated outlet temperatures show a difference. The simulation with the uniform inlet profile predicts a later increase of the temperature at the outlet face and afterwards a steady temperature increase. The simulations based on the uneven velocity distribution predict an earlier increase of the temperature and show in the range of 50 - 80 s a more dynamic unsteady behavior. Only marginal differences in the outlet temperature development of the three "profile" simulations occur.

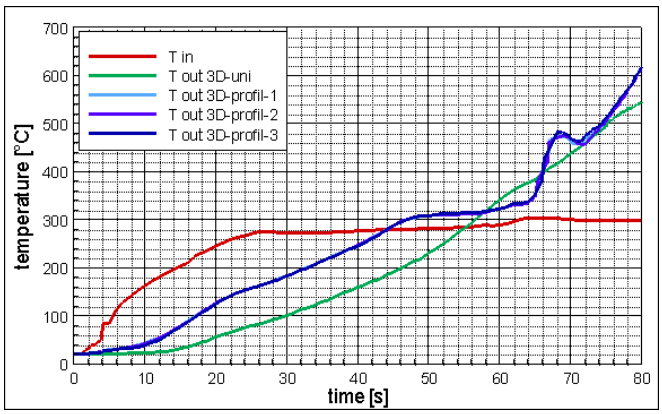

Fig. 5 Inlet and calculated outlet gas phase temperatures during the first 80 s of the cycle

GLOBAL SPECIES CONVERSION

In Fig. 6 - Fig. 8 the simulation results for the transient development of the conversion of the exhaust gas species CO, NO and total hydrocarbons (THC) are shown. All diagrams show a distinct difference between the simulation based on the uniform inlet conditions on the one hand and the simulation based on the uneven inlet conditions on the other hand. Although the time to light-off does not substantially differ between the different simulations (CO: 41 - 43 s, THC: 40 - 42 s, NO: 39 - 41 s), the simulation based on the uniform velocity profile predicts a rather steady increase of the conversion rate thereafter. In contrast, the simulations based on the velocity profile shown in Fig. 4 show an intense decrease of the conversion rate of all species during the period between 50 and 70 seconds. The conversion rates of CO and NO drop to below 40 % again. Only after 70 seconds from start-up the simulations based on the non-uniform inlet conditions also show a steady increase and they approach the results based on the even inlet velocity distribution. Looking at the mean inlet conditions during this period of time (Fig. 9), the reason for the decrease of the conversion rates must be the increase in the mean inlet velocity.

The predictions of the conversion rates reveal slight differences between the different "profile" simulations. They are particular obvious for THC at the time steps of 48 s and for CO additionally at the time step of 60 s. Obviously, under the given temperature and mass flow conditions, a finer resolution of the monolith concerning the number of channels to be simulated yields in a different and presumably better simulation result. On the other hand, a lager number of single channel simulations during one time step requires a higher computational capacity.

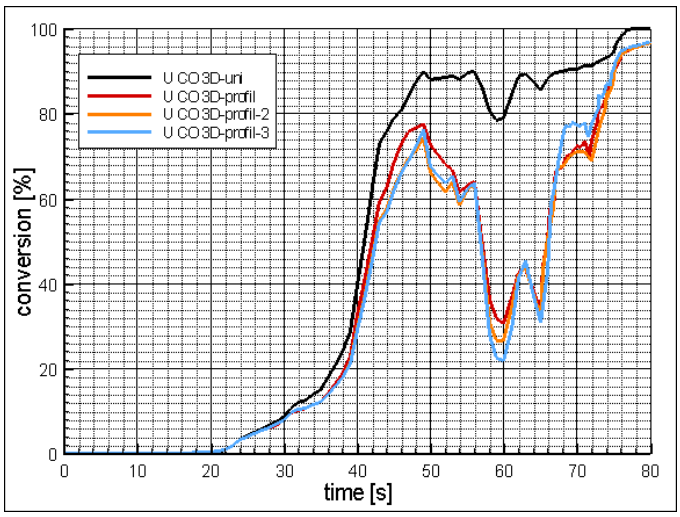

Fig. 6 Predicted CO conversion

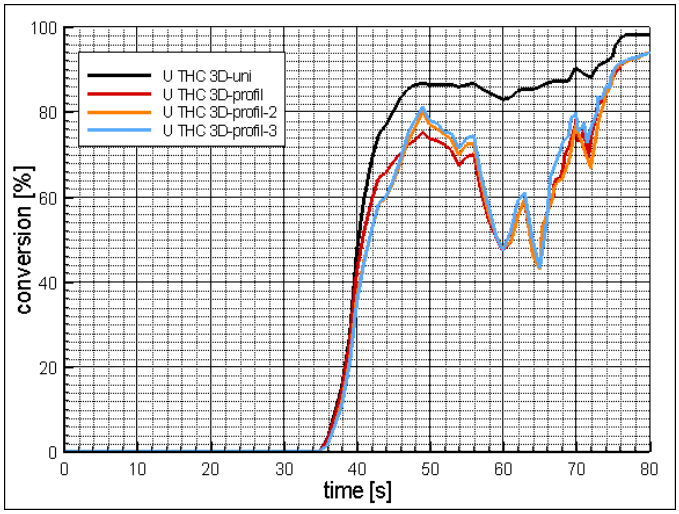

Fig. 7 Predicted THC conversion

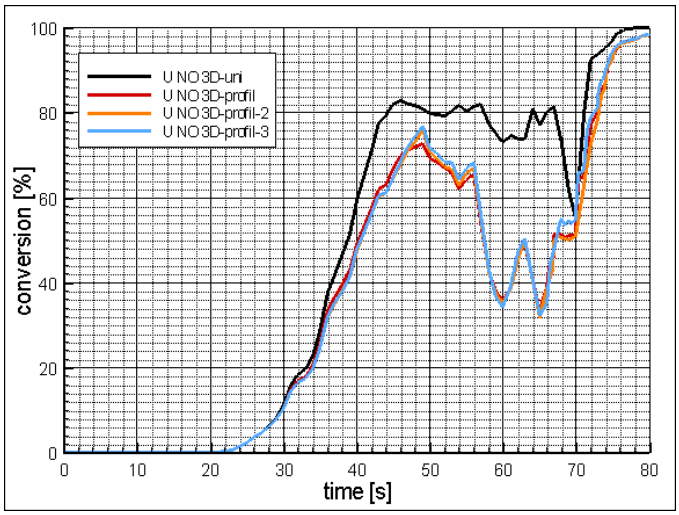

Fig. 8 Predicted NO conversion

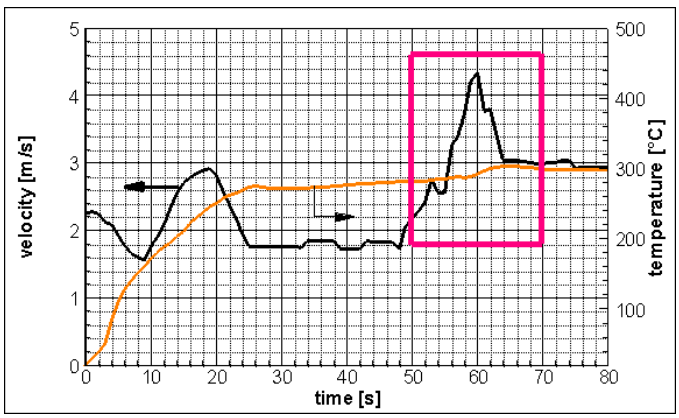

Fig. 9 Gas phase temperature and mean velocity at the inlet

TEMPERATURE DISTRIBUTIONS IN THE MONOLITH

The temperature distributions in the monolith reveal the differences more clearly. Although at the time step of 40 s after start-up the conversion rates do not differ substantially, not only show the mean temperature at the outlet (see Fig. 5), but also the temperature profile in the monolith distinct differences. Fig. 10 shows that the temperature profile in the monolith is relatively even and symmetrical with a steady increase of the temperature near the inlet of the monolith, due to heat of reaction. Behind the reaction zone the temperature decreases steadily again.

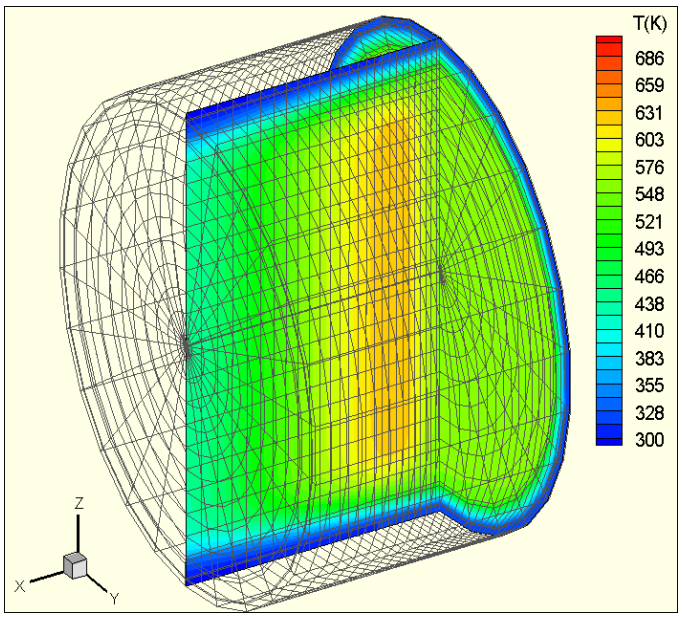

Fig. 10: Temperature profile in the monolith 40s after start-up; uniform inlet flow distribution

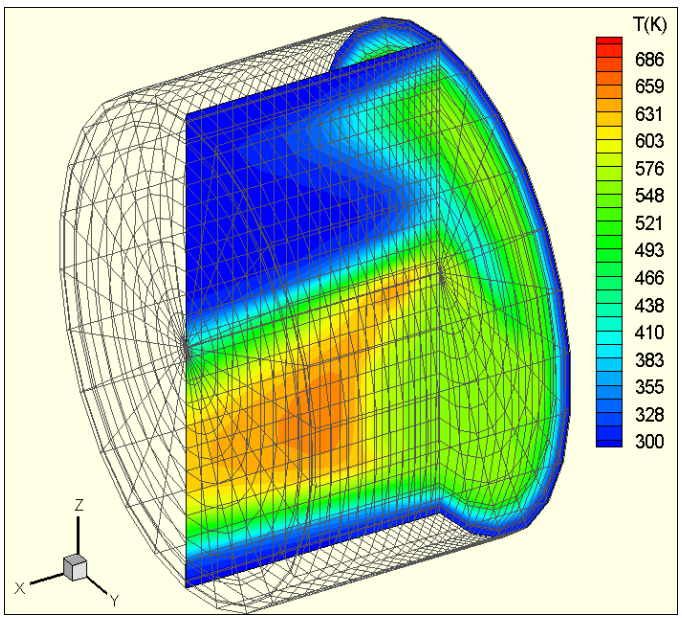

Fig. 11: Temperature profile in the monolith 40 s after start-up; inlet flow distribution as shown in Fig. 4

In contrast, the simulation based on the uneven velocity distribution shows a totally different image. The temperature profile in the monolith is highly asymmetric with a hot zone in the lower and a large cold zone in the upper part of the monolith (referring to the orientation of Fig. 10 and Fig. 11).

These differences in the temperature profile in the monolith occur in the same way during the time step of 60 s as shown in Fig. 12 and Fig. 13.

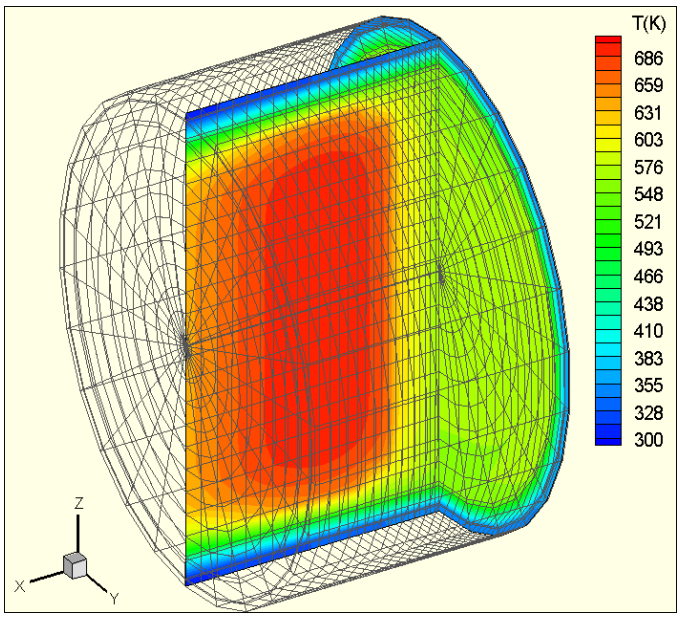

Fig. 12: Temperature profile in the monolith 60 s after start-up; uniform inlet flow distribution

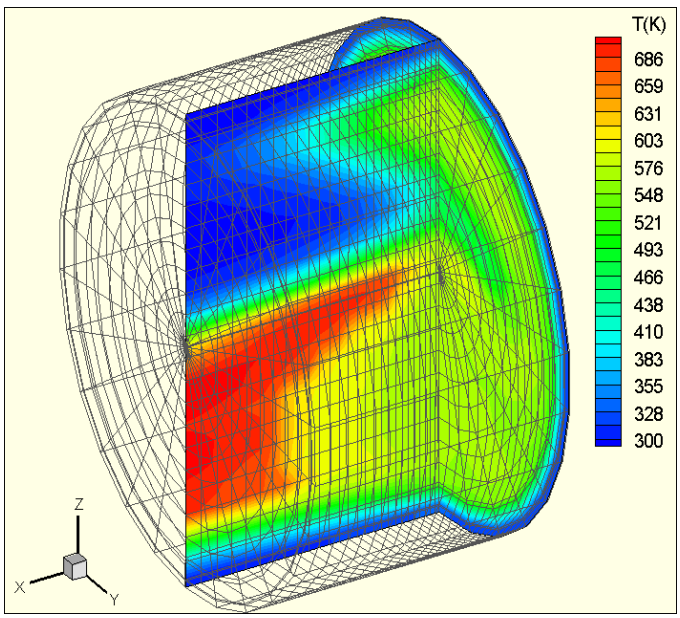

Fig. 13 Temperature profile in the monolith 60 s after start-up; inlet flow distribution as shown in Fig. 4

DISTRIBUTION OF THE CONVERSION EFFICIENCY

The following results concentrate on the conversion at the time step 40 s after start-up for the distributed inlet velocity profile. For the interpretation of these results the temperature profile is essential. Therefore, additional to the results depicted in Fig. 11 the temperature profile at the inlet and at the oulet face are shown in Fig. 14 and Fig. 15.

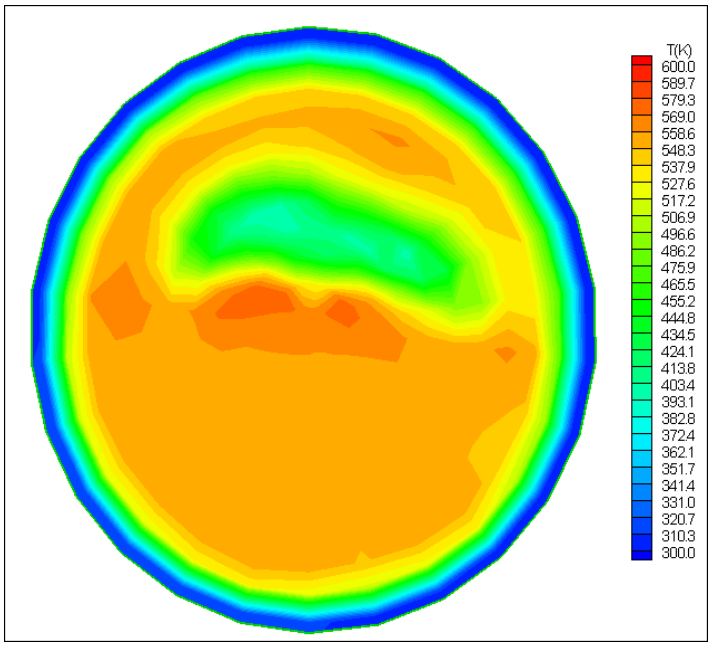

Fig. 14: Temperature profile at the inlet of the monolith 40s after start-up

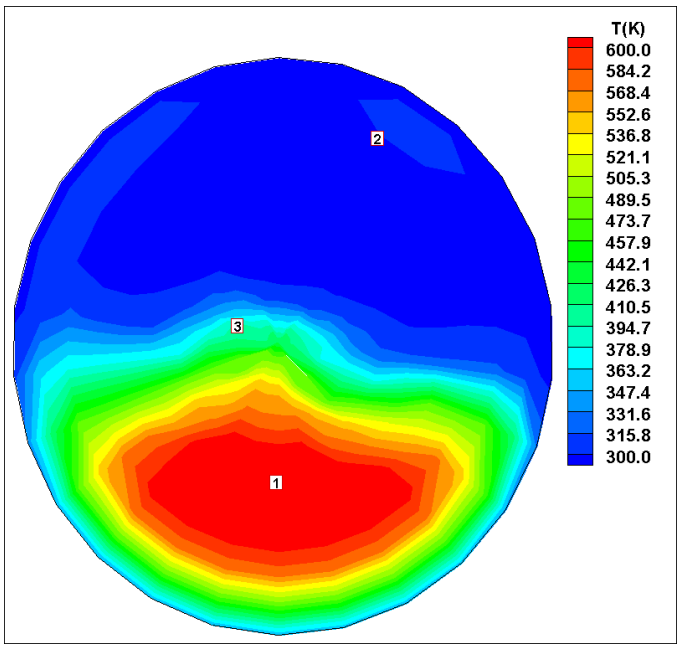

Fig. 15: Temperature profile at the outlet of the monolith 40s after start-up
For the marked positions 1, 2 and 3 single channel simulation results are presented

In Figs. 16 – 18, the distribution of the conversion of THC, CO and NO is shown. It is obvious that the distributions resemble each other. In the center of the monolith there are two regions with a very high conversion of all species. The maximum conversion detected here are for THC 89.1%, for CO 76.1% and for NO 86.6%. But while THC is converted almost only in the lower part of the monolith (referring to the orientation in Fig. 16 - Fig. 18), CO and NO show in the upper part of the monolith a low conversion, too.

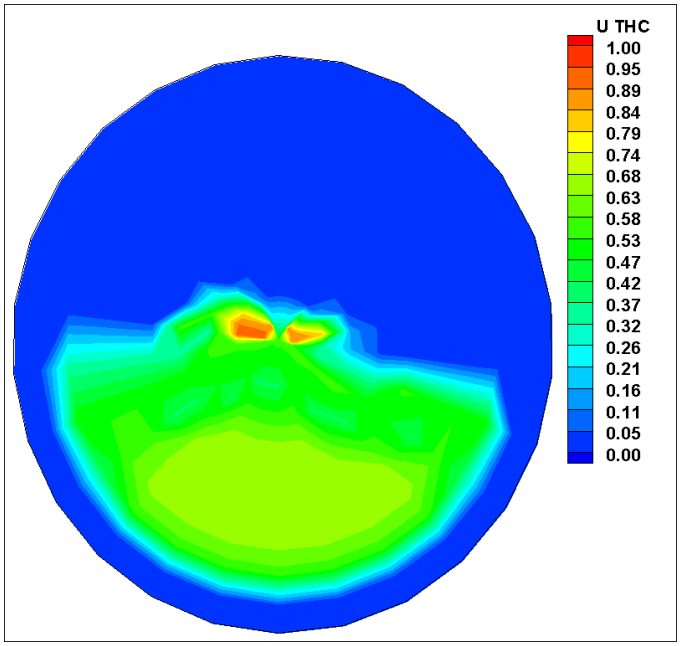

Fig. 16: Distribution of the THC conversion efficiency across the monolith 40s after start-up

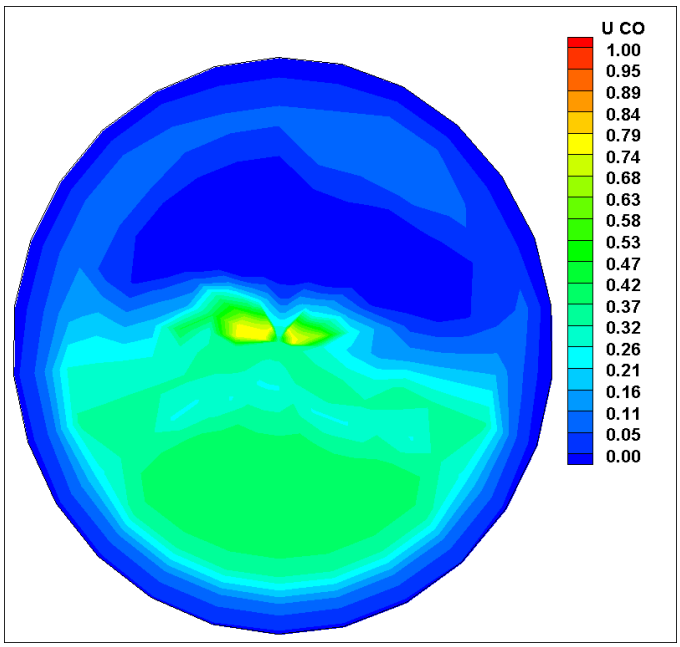

Fig. 17: Distribution of the CO conversion efficiency across the monolith 40s after start-up.

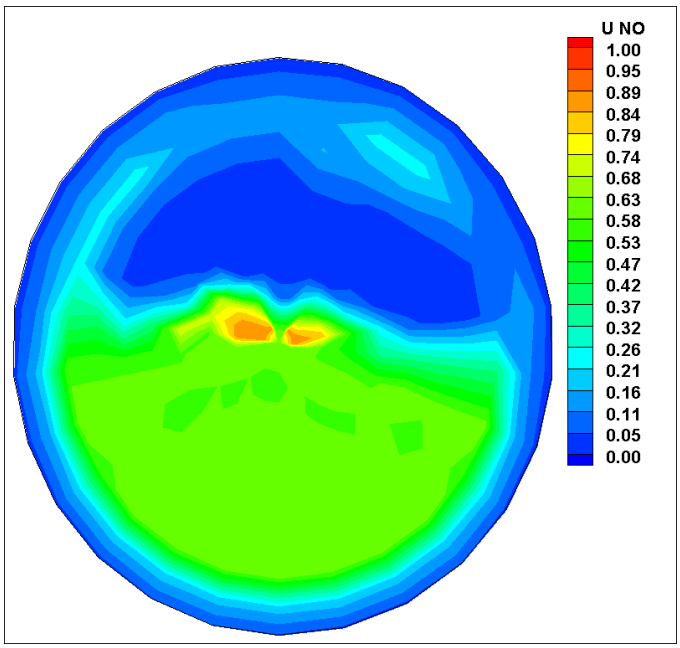

Fig. 18: Distribution of the NO conversion efficiency across the monolith 40 s after start-up.

In Fig. 15 three positions are marked: at these points the results will be examined in more detail. Single channel simulation results from the code DETCHEM^{CHANNEL} enable to learn more about the processes occurring in the monolith at these position (Fig. 20 - Fig. 22) . Additionally the wall temperatures along the channels are presented in Fig. 19. It is obvious that the thermal boundary conditions for the channels at the three different positions in the monolith are completely different. In channel 2 the temperature is steadily decreasing. The maximum temperature (562 K) is only slightly higher than the inlet temperature (550 K). In channels 1 and 3 temperatures of 656 K and 643 K are reached. In channel 3 the temperature is increasing in the first fifth of the channel, and after reaching the maximum temperature, steadily decreasing until it reaches a temperature at the outlet of approximately 400 K. Channel 1 shows a different temperature profile. At the entrance, the temperature increases only slightly. After the first quarter of the channel length, it increases faster and reaches the maximum in the middle of the channel. The following decrease of the temperature is much slower than in the other two channels.

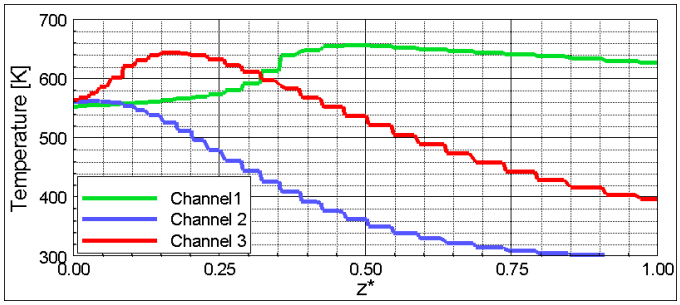

Fig. 19: Distribution of the wall temperatures of the channels along the monolith; z* is the relative axial coordinate, i. e. z/z_{ges}

Furthermore, the different flow velocities inside the channels have to be taken into account. In Tab. 2 the gas phase velocities at the inlet of the channels and the over-all conversion rates of the species THC, NO and CO are listed.

	channel 1	channel 2	channel 3
gas phase velocity at the inlet	9.22 m/s	0.99 m/s	1.85 m/s
over-all conversion THC	0.662	0.042	0.846
over-all conversion NO	0.603	0.233	0.832
over-all conversion CO	0.401	0.103	0.681

Tab. 2: Overview over the gas phase velocity at the entrance and the over-all conversion rates of the three channels

The conversion in channel 1 is relatively low concerning the relatively high wall temperatures. The reason for this is the high gas phase velocity in the channel. This leads to mass transfer limitation. The distribution of the conversion rate of the species confirms this assumption (Fig. 20).

In channel 2 the temperature is still too low and only some NO is converted (Fig. 21).

In channel 3 the temperatures are sufficiently high and the mass flow sufficiently low for significant conversion (Fig. 22). It is also shown that the conversion is not mass transfer limited but kinetically limited. Here only an increase of the temperature in the monolith would lead to higher conversion.

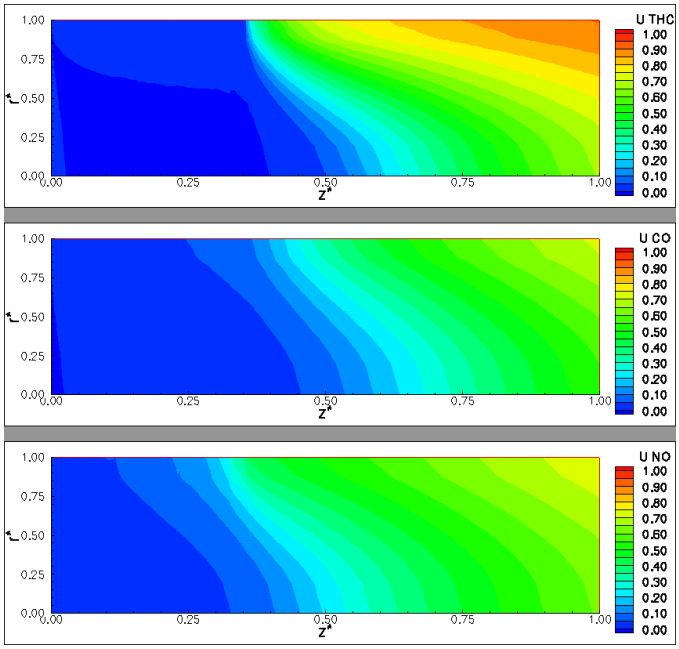

Fig. 20: Distribution of species conversion rates along a single channel at position 1, 40s after start-up
top: THC conversion rate,
middle: CO conversion rate,
bottom: NO conversion rate

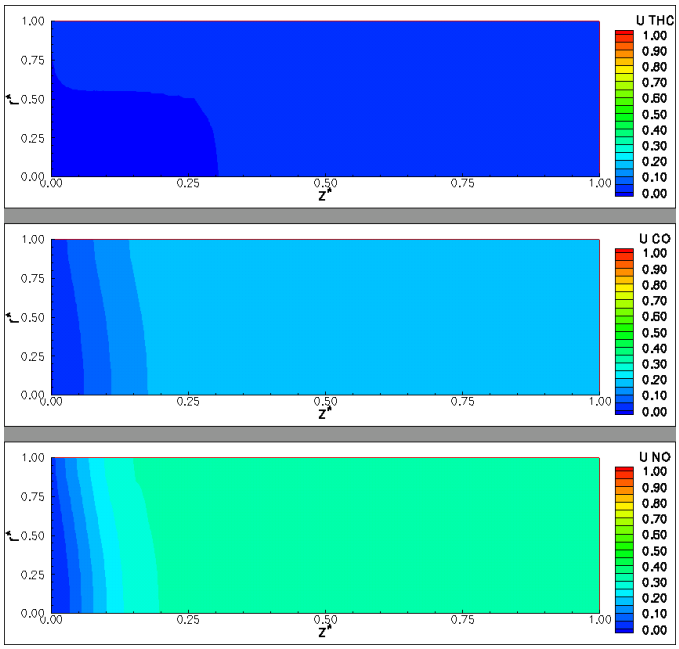

Fig. 21: Distribution of species conversion rates along a single channel at position 2, 40s after start-up
top: THC conversion rate,
middle: CO conversion rate,
bottom: NO conversion rate

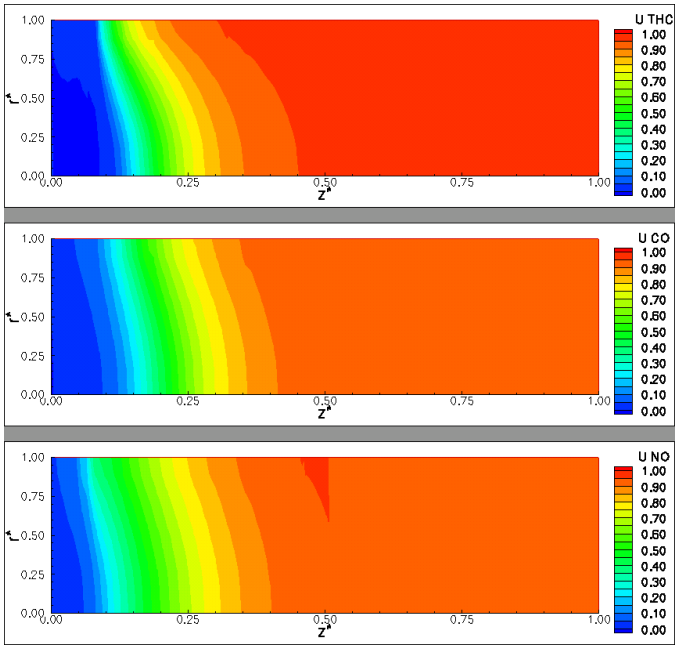

Fig. 22: Distribution of species conversion rates along a single channel at position 3, 40s after start-up
top: THC conversion rate,
middle: CO conversion rate,
bottom: NO conversion rate

CONCLUSION

The results reveal unequivocally the negative influence of a velocity maldistribution in front of the catalytic converter on the conversion efficiency in the first minutes of the test cycle. Although a smaller part of the converter is heated up faster and is lit off earlier than the rest of the monolith, the overall conversion is lower than in the case of the even velocity distribution.

A good estimation of the influence of the velocity profile on the transient behavior of the catalyst is possible using a relatively low number of channels simulated. The chosen representative channels may vary significantly without loss in the prediction quality. Channels with extreme inlet conditions and wall temperatures mainly determine the behavior of the monolith.

In future, we will use the code DETCHEM^{MONOLITH} for a more detailed analysis of the exhaust gas system, which is coupled to CFD simulations of the up-stream tail-pipe flow.

ACKNOWLEDGEMENTS

The authors would like to thank Laurence Marie for providing data used as inlet conditions. Further we like to acknowledge the contributions of Chrys Correa, Daniel Chatterjee and Luba Maier to the development of the simulation tools and models.

REFERENCES

/1/ DETCHEM, Version 1.5, O. Deutschmann, C. Correa, S. Tischer, D. Chatterjee, S. Kleditzsch, J. Warnatz, IWR, Universität Heidelberg, *http://reaflow.iwr.uni-heidelberg.de/~dmann/DETCHEM.html*

/2/ Th. Hauber, P. Zacke, J. Braun, D. Ueberschär: "Influence of the Space between Monoliths and the Geometry of Endcones on the Conversion Rate of a Catalytic Converter"; SAE 980424

/3/ A.P. Martin, N. S. Will, A. Bordet, P. Cornet, C. Gondoin, X. Mouton: "Effect of Flow Distribution on Emissions Performance of Catalytic Converters"; SAE 980936

/4/ R.E. Hayes, S.T. Kolaczkowski, W.J. Thomas: "Finite Element Model for a Catalytic Monolith Reactor"; Computers Chem. Eng. 16, 654-657 (1992)

/5/ R.E. Hayes, S.T. Kolaczkowski: "Introduction to Catalytic Combustion"; Gordon & Breach Publishing Group (1998)

/6/ S.T. Kolaczkowski: "Modelling catalytic combustion in monolith reactors – challenges faced"; Cataysis Today 47, 209-218 (1999)

/7/ R.E. Hayes, S.T. Kolaczkowski: "A study of Nusselt and Sherwood numbers in a monolithic reactor"; Catalysis Today 47, 295-303 (1999)

/8/ R. Jahn, D. Snita, M. Kubicek, M. Marek: "3-D modelling of monolith reactors"; Catalysis Today 38, 39-46 (1997)

/9/ G.C. Koltsakis, P.A. Konstantinidis, A.M. Stamatelos: "Development and application range of mathematical models for 3-way catalytic converters"; Applied Catalysis B: Environmental 12, 161-191 (1997)

/10/ J. Braun, Th. Hauber, H. Többen, J. Windmann, Peter Z. , D. Chatterjee , C. Correa , O. Deutschmann, L. Maier, S. Tischer, J. Warnatz : "Three-Dimensional Simulation of the Transient Behavior of a Three-Way Catalytic Converter"; SAE 2002-01-0065

/11/ S. Tischer, C. Correa, O. Deutschmann: "Transient three-dimensional simulations of a catalytic combustion monolith using detailed models for heterogenous and homogenous reactions"; Catalysis Today 69, 57-62 (2001)

/12/ R. Jahn, D. Snita, M. Kubicek, M. Marek, "3-D modeling of monolith reactors", Catalysis Today 38, 39 (1997)

/13/ L.L. Raja, R.J. Kee, O. Deutschmann, J. Warnatz and L.D. Schmidt, "A Critical Evaluation of Navier-Stokes, Boundary-Layer and Plug-Flow Models of the Flow and Chemistry in a Catalytic-Combustion Monolith", Catalysis Today 59, 47 (2000)

/14/ I. Mantzaras, C. Appel, P. Benz, U. Dogwiler, "Numerical modeling of turbulent catalytically stabilized channel flow combustion", Catalysis Today 59, 3-17 (2000),

/15/ P. Deuflhardt, E. Hairer and J. Zugk, "One-Step and Extrapolation Methods for Differential-Algebraic Systems", Num. Math. 51, 501 (1987)

/16/ Tecplot® User's Manual Version 9, Revision 2, Amtec Engineering, Inc. Bellevue, Washington (2001)

/17/ FLUENT 6.0, Fluent Inc., Lebanon, NH (2001)

/18/ D. Chatterjee, O. Deutschmann, J. Warnatz, "Detailed surface reaction mechanism in a three-way catalyst", Faraday Discussions 119 (2001), 371-384

NOTATION

c_i	concentration
c_p	specific heat
f_k	coverage dependency function
h_i	enthalpy of species *i*
h	enthalpy of the mixture
p	pressure
q	heat source term
j_i	diffusive flux including surface flux
k_{fk}	reaction rate
r	radial spatial coordinate
A	face area
A_k	pre-exponential factor
E_{ak}	activation energy
$F_{cat/geo}$	ratio of catalytic to geometric surface area
K_s	number of surface reactions
M_i	molar Mass
N_g	number of gas-phase species
N_s	number of surface species
R	gas constant
T	temperature
t	time
u	axial velocity
v	radial velocity
w	normal velocity
$\overline{w}$	mean normal velocity
Y_i	mass fraction of species *i*
z	axial spatial coordinate
β_k	temperature exponent
ε_{ik}	coverage dependent change of activation energy
η	washcoat effectiveness factor
λ	thermal conductivity
γ	uniformity index
μ	viscosity

μ_{ik} coverage dependent change of reaction order
ν_{ik} stoichiometric coefficients
ρ density
σ channel density
Θ_i surface coverage